Gianmario Scotti, Petri Kanninen, Tanja Kallio, and Sami Franssila, "Bulk-Aluminum Microfabrication for Micro Fuel Cells," J. Microelectromech. S., doi:10.1109/JMEMS.2013.2274592. © 2013 IEEE. Preprinted by permission of IEEE.

This article has been accepted for inclusion in a future issue of this journal. Content is final as presented, with the exception of pagination.

Bulk-Aluminum Microfabrication for Micro Fuel Cells

Gianmario Scotti, Petri Kanninen, Tanja Kallio, and Sami Franssila

***Abstract*— We present a simple method for microfabricating microfluidic devices by wet etching of bulk aluminum wafers. Aluminum wafers are identical to silicon wafers in terms of dimensions and can easily be processed in standard clean room processes like lithography, etching, and thin film deposition. Aluminum thin film wet etching in phosphoric acid-based etchants is well established. In this paper, it is extended to much greater depths than before. 80 μm deep structures have been fabricated. A hydrogen-fueled micro fuel cell has been microfabricated from bulk aluminum. These fuel cells achieved very high current densities of 1.1 A cm^{-2} and power density up to 228 mW cm^{-2}. Considering the simplicity of bulk aluminum micromachining, these results are very encouraging. [2013-0157]**

***Index Terms*— Aluminum, hydrogen, micro fuel cell, micromachining, microfluidics, etching.**

I. Introduction

WHILE silicon is the most common substrate material for microfabrication, others are routinely used: glass [1], fused silica [2], various polymers [3], alumina [4], and photostructurable glass-ceramics [5]. Applications of bulk aluminum wafers remain rare: microneedles have been made by a combination of aluminum dicing and wet etching [6].

Aluminum wafers are used in microelectronics cleanrooms as vehicles for testing robotic wafer handling, because they are ductile, and much less prone to breakage than brittle silicon wafers.

Aluminum wafer mechanical specifications (diameter, thickness, TTV, even flats) are similar to those of silicon, ensuring compatibility with microfabrication equipment. The maximum temperatures that these wafers can tolerate is ca. 450 °C, making most thin film deposition processes available. Pure aluminum is very soft (15 HB Brinell hardness) and a harder alloy, such as 6061 (95 HB), is desirable when used as a bulk material. The alloying elements for 6061 include copper (0.15-0.4%), iron (0.7%), silicon (0.4-0.8%), magnesium (0.8-1.2%), zinc (0.25%) etc. The presence of these alloying elements necessitates that etching be performed in a dedicated container to avoid metallic contamination spreading in the cleanroom. Wafers made from other aluminum alloys are also available. Table 1 summarizes the specifications of the aluminum wafers used in this work.

TABLE I
ALUMINUM WAFER SPECIFICATIONS

Material	6061-T6
Diameter	100 mm
Thickness	813 μm
Thickness tolerance	75 μm
Polished side roughness	30 nm
Non-polished side roughness	5 μm
Anodization	none
Bow/Warp	< 100 μm

Aluminum is highly conductive ($\rho \approx 3$ $\mu\Omega$-cm), which is a major benefit in applications where resistive losses have to be minimized. Aluminum is, however, easily oxidized, just like silicon, and the surface is most often covered by a layer of native Al_2O_3. Anodized aluminum wafers are also available, with oxides of various thickness, up to several tens of μm. Depending on application, this aluminum oxide can be used to benefit or it has to be removed before processing.

Aluminum etching in phosphoric acid-based solutions is well known [7]. For micromachining bulk aluminum, wet etching is the preferred choice because reactive ion etching (RIE) of aluminum in chlorine plasmas has a similar etch rate ($\sim$1 μm/min) but poor mask selectivity which limits etched depths to a few micrometers. Obviously wet etching is limited to isotropic profiles. Aluminum has been etched electrochemically to produce thick (e.g. 40 μm) high aspect ratio structures (e.g. 1000:1) [8]. Aluminum foils are used as starting material, not wafers. Besides, the electrochemical pore etching is not a general-purpose fabrication process, but limited to certain shapes and sizes only.

Fuel cells are electrochemical energy conversion devices, which transform chemical energy into electrical energy [9]. They are composed of two flowfields in which fuel and oxidant flow, separated by a solid or liquid electrolyte (Fig. 1). A membrane-electrode assembly (MEA) is inserted between the flowfields. MEA consists of proton-conductive polymer (Nafion®). Nafion® is often covered by platinum or PtRu catalyst to facilitate the oxidation/reduction reactions. Fuel cells often use a gas diffusion layer (GDL) to aid gas dispersion and diffusion, and oxidation product removal.

Manuscript received April 9, 2013; revised July 2, 2013; accepted July 22, 2013. This work was supported by the IPPES project (MIDE foundation, Aalto University, Finland) and the CHEMSEM graduate school. Subject Editor Y. Zohar.

G. Scotti and S. Franssila are with the Department of Materials Science and Engineering, Aalto University, Espoo FI-00076, Finland (e-mail: gianmario.scotti@gmail.com; sami.franssila@aalto.fi).

P. Kanninen and T. Kallio are with the Department of Chemistry, Aalto University, Espoo FI-00076, Finland (e-mail: petri.kanninen@aalto.fi; tanja.kallio@aalto.fi).

Color versions of one or more of the figures in this paper are available online at http://ieeexplore.ieee.org.

Digital Object Identifier 10.1109/JMEMS.2013.2274592

1057-7157 © 2013 IEEE

This article has been accepted for inclusion in a future issue of this journal. Content is final as presented, with the exception of pagination.

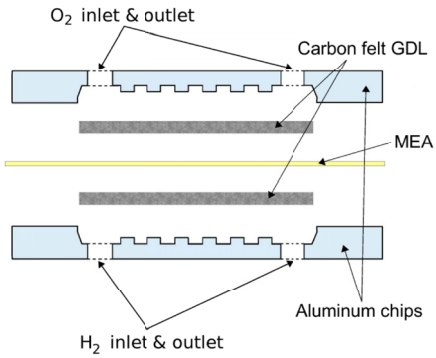

Fig. 1. Construction of a bulk-aluminum micromachined MFC with carbon felt gas diffusion layer (GDL) inserted in the basins and a Nafion MEA in the middle.

Micro fuel cells (MFC) are microfluidic devices produced by microfabrication [10].

In micro fuel cells, a highly electrically conductive bulk material is a desirable feature, because the flowfield can also act as a current collector. Highly-doped silicon has been used to accomplish this [11], [12]. Even higher conductivity than with highly doped silicon can be achieved with metals: for instance, in [13] screen-printed and sintered nickel was used as a substrate for a micro solid oxide fuel cell (SOFC).

In this paper we present micro fuel cells fabricated by deep aluminum wet etching, with 80 μm maximum etched depth. Fuel cell characterization shows that bulk aluminum is an attractive material for this application.

II. Experimental

A. Aluminum Micromachining

We carried out all processing using 6061 aluminum alloy wafers using phosphoric acid-based wet etching. A 813 μm thick, single-side polished (average roughness below 30 nm) 100 mm diameter aluminum wafer was the starting point. The wafer was not anodized; no alumina, apart from a native oxide layer, was present.

The initial step was priming using HMDS, for better adhesion of photoresist. After priming, photoresist such as AZ 5214E or AZ 4562 was spinned at 4000 RPM. The obtained photoresist thickness was 1.4 μm when using AZ 5214E, and 6.2 μm when using AZ 4562. Resist spinning was followed by a softbake in a 90 °C oven for 30 minutes, alignment and exposure (mask aligner Süss MicroTec®MA 6) to pattern the resist. The developer used was MicroChemicals GmbH AZ 351B in a 1:5 de-ionized (DI) water dilution.

After development, the wafer was hard-baked at 120 °C on a hotplate for 1 to 3 minutes, depending on the resist thickness.

The etchant used was a phosphoric acid-based commercial etchant, Honeywell PWS 80-16-4 (65), a water solution of 74% H_3PO_4 and 2.5% HNO_3. The etching was performed in a dedicated glass beaker, to avoid contamination. The beaker was placed on a hotplate with separate thermal sensor immersed in the etching solution. The temperature was set at 50 °C.

After etching, the wafer was subjected to a water jet to remove the dark gray patina formed on the etched surface. The water jet would also remove any overhanging resist at the edge of the etched structures. Final resist strip was performed in an ultrasound acetone bath, followed by short baths in clean acetone and isopropanol.

A series of experiments was performed to determine the etch rate of 6061 aluminum under various conditions. A test pattern, consisting of stripes (10-80 μm wide) and large squares (1 $\times$ 1 cm^2) were used to pattern the polished side of the wafers (Table 2). Wafers with smaller features were etched 5, 10, 20 and 35 minutes and the wafers with large squares were etched 20, 50 and 80 minutes, to determine the etching behavior in longer time scales, as well as the surface roughness evolution. Etched depth and surface roughness were characterized using a Veeco Dektak V200-Si stylus profilometer (12.5 μm radius of curvature of tip) and a Wyko SP3000W optical profilometer.

TABLE II
Summary of Etch Test Structures

Mask opening	Shape	Size (side or width) [μm]	Distance between structures [μm]
Channel 1	Stripe	10	50
Channel 2	Stripe	20	100
Channel 3	Stripe	40	200
Channel 4	Stripe	80	400
Basin	Square	1x1 cm^2	2000

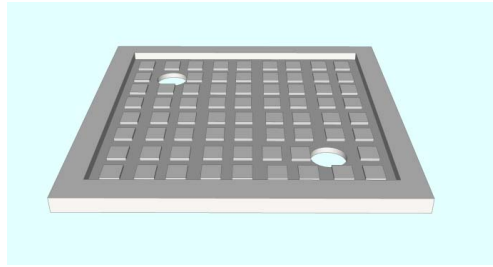

Fig. 2. 3D model of one aluminum MFC chip showing the 80 μm deep basin filled with 30 μm high square-shaped flow field structures. Gases are inserted through diagonally placed drilled inlet holes.

B. MFC Microfabrication and Assembly

A 3D model of the desired structure of the chips can be seen on Fig. 2. This structure is identical to a silicon design published earlier [12]. As can be seen from Figures 1–3, the MFCs have a recessed flowfield, i.e., a flowfield at the bottom of a basin. The basin allows for the integration of carbon felt gas diffusion layer (GDL), as shown in Fig. 1. Two masks and two etching steps are required in the process–one each for the basins and the flowfields.

This article has been accepted for inclusion in a future issue of this journal. Content is final as presented, with the exception of pagination.

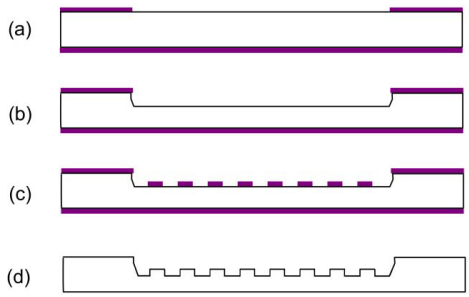

Fig. 3. Microfabrication flow of MFC chips with backside resist protection: (a) spinning resist and patterning the front; (b), wet etching to form the basins; (c) spinning new resist on the front and patterning for flowfield; (d) etching to form the flowfield and resist stripping.

MFC chip microfabrication steps are shown in Fig. 3. The main steps are:

(a) After priming, photoresist was spinned on both sides of the wafer. This was followed by a softbake, and lithography steps to pattern the resist on the polished (front) side of the wafer. The first mask defines the areas of the basins. Backside is protected by photoresist.
(b) The basins were etched as described in the previous subsection, for 50 minutes to obtain $\sim$ 50 μm depth.
(c) Lithography was repeated on the front side using the flowfield mask, to form a grid pattern on the bottom of the basins. The flowfield grid consists of 50 μm wide stripes at a 300 μm pitch. This step required spinning resist on an already patterned wafer (50 μm deep basins). In order to obtain a uniform coating, 4 ml of resist was applied before spinning, sufficient to almost entirely cover the wafer. After spinning, a continuous layer covering all features, was obtained with both AZ 5214 and AZ 4562 resists.
(d) The flowfield target depth was 35 μm (ca. 30 minutes etch time). The resist was removed with acetone and 40 nm of chromium was sputtered on the front of the wafer, to protect it against corrosion and oxidation. Gas inlet holes were drilled using a 400 μm diameter drill bit.

The chips were diced apart in a dicing saw normally used for silicon wafer dicing. A Micro-Swiss hubless diamond blade (55 mm outside diameter, 250 μm thick) with nickel binder was used. The blade was rotating at 15000 RPM and had a 0.5 mm/s feed rate.

The MFCs were assembled by inserting a carbon cloth GDL in the basins, and sandwiching a membrane-electrode assembly (MEA) between two aluminum chips (Fig. 1).

The MEA was commercial Gore Primea®, with Pt loading of 0.3 mg cm^{-2} on the cathode (oxidant) and 0.1 mg cm^{-2} on the anode side (fuel) and carbon felts (E-Tek ELATL®T1200N) were used as GDLs.

C. Fuel Cell Characterization

The performance of the MFCs was characterized by clamping them in a measurement jig [11], [12] with gas fittings and electrical contacts. The plates of the jig were made of aluminum, so electrical contact with the chips is directly realized.

Polarization curves were measured by sweeping the cell potential from open circuit voltage to 0.05 V and measuring the current produced with a Metrohm Autolab PGSTAT100 potentiostat equipped with BSTR10A booster to manage currents over 0.3 A. The potential was swept at 3 mV s^{-1} with 1 mV steps. Hydrogen (5.0, Aga, Finland) was used as the fuel and oxygen (5.0, Aga, Finland) and artificial air (80% nitrogen, 20% oxygen, 5.0, Aga, Finland) as the oxidant. Long term stability of the cell was studied with a chronoamperometric measurement, where the potential was kept at 0.6 V for 12 h and the produced current was measured. Only oxygen was used as the oxidant in this measurement. All the gases were humidified and fed at 50 ml min^{-1}. All the measurements were made at room temperature.

TABLE III
CHANNEL ETCH RESULTS

Etch time [min]	Channel 1 [μm]	Channel 2 [μm]	Channel 3 [μm]	Channel 4 [μm]
5	4.9	4.9	5.1	5.2
10	10.4	11.2	11.7	12.5
20	20.0	23.5	23.8	23.8
35	28.1	33.4	35.2	36.2

III. RESULTS AND DISCUSSION

A. Aluminum Micromachining

Table 2 lists the test patterns used in the aluminum wafer etching experiments. The distinction between "stripe" and "channel" is made here, because the final width of the channel is larger than the width of the width of the mask opening. As it will be shown, both the width and the depth of the channels are influenced by the width of the mask opening.

The structures were patterned with positive polarity. That is, after etching, the stripes became channels and the squares become square basins.

Etched depth results from Dektak stylus profilometer measurements are shown in Table 3. Since the bottom of the channels was curved and narrow, and the stylus tip relatively large, average step height (ASH) was not measured; instead for every channel the lowest point was measured, and the result averaged over a large number of measurements.

Based on these measurements, we calculated the etch rate for each mask opening width and etch time, and summarized them in Fig. 4.

Two phenomena are eminent from these graphs: one is the fact that with narrower channels (narrower mask openings), the etch rate will be smaller. This is unsurprising, considering that the active species from the etchant have to diffuse through a narrower aperture towards the aluminum surface. If the aperture in the photoresist is sufficiently small it will affect the diffusion ([14] chapter 13). H_3PO_4:HNO_3-based etching of aluminum is a fast, exothermic reaction and is therefore diffusion-controlled.

This article has been accepted for inclusion in a future issue of this journal. Content is final as presented, with the exception of pagination.

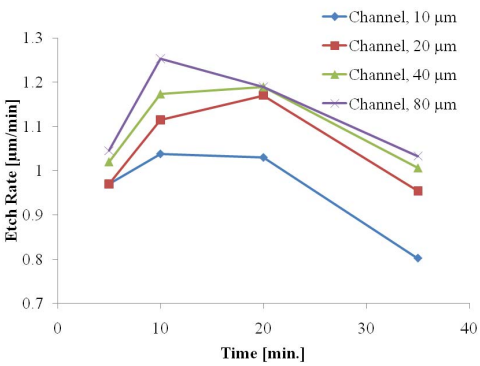

Fig. 4. Etch rates of the various channels as a function of etch time. After 20 minutes of etching, the etch rate starts to decrease. Also, narrower channels etch slower than wider ones.

TABLE IV
SUMMARY OF 1 × 1 cm^2 BASIN ETCH RESULTS

Etch time [min]	Etch depth [µm]	Calculated etch rate [µm/min]	Roughness (Dektak) [nm]	Roughness (Wyko) [nm]
20	18.9	0.94	436	706
50	43.7	0.87	677	805
80	66.4	0.83	826	967

The second phenomenon is less expected; namely, that the etch rate for a given type of pattern, will decrease as the etching progresses over 10 to 20 minutes. We hypothesize that the alloying elements, some of which are not etched in the phosphoric acid-based etchants, form a barrier (i.e. the dark gray patina mentioned earlier), and as etching progresses this barrier becomes thicker and becomes an obstacle for etching. The effect is similar to deep wet etching of Pyrex glass wafers, where SiO_2 is etched by HF, whereas the metallic oxides present in the glass are not [15].

To verify the etch rate decrease phenomenon in 6061 aluminum etching, we prepared samples with relatively very large open patterns; 1 × 1 cm^2 squares, in which case we assume that all aspect ratio and resist undercut phenomena can be neglected and the measured etch rate depends only on diffusion through the etch by-products. These large etched areas were suitable also for computing average step height (ASH) and for measuring the surface roughness. Average roughness (Ra) and root mean square of roughness (Rq). Ra and Rq were measured with both the Dektak and the Wyko devices. ASH was only measured with the Dektak stylus profilometer.

The results of large basin experiment are summarized in Table 4. The slow-down of etch rate is confirmed, and after 80 minutes it is as low as 0.83 μm/min. Ra and Rq both increase with etch time, regardless whether measured with the stylus or optical profilometer. This, too, is similar to glass etching with different HF-based etchant compositions [16]. Obviously, the relatively large radius of curvature of the stylus tip will understate the roughness. It is worth bearing in mind that, since we used ASH to determine the step height, unlike with the channels, the etch depth is somewhat smaller.

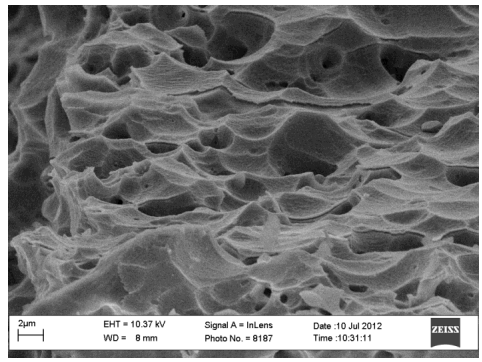

Fig. 5. SEM of etched 6061 aluminum surface (etch time 50 min). Very significant roughness is visible.

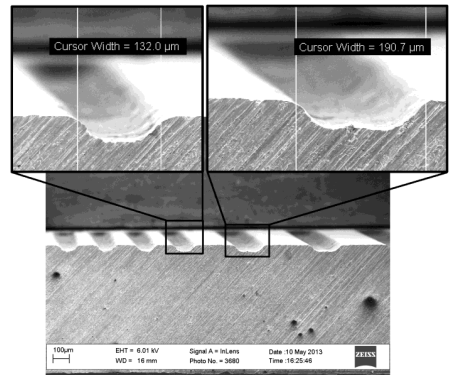

Fig. 6. SEM micrographs of Channel 3 (on the left) and Channel 4 (on the right) ∼ 35 μm deep test structures (etched 35 min. at 50 °C). Channel 3 were obtained with a mask aperture width of 40 μm, whereas Channel 4 were obtained with a 80 μm width. The resulting channels are more than 130 and 190 μm wide, respectively.

Scanning electron microscopy (SEM) images of the etched chips were made to analyze the etched surfaces and microstructures. As can be seen in Fig. 5, the etched surface roughness is sizable, yet small compared with etched depths (ca. 1% only).

Cross sectional SEMs of etched structures were prepared by dicing because fracture is not possible for ductile polycrystalline metal. To prepare the samples for SEM characterization, a cut was made near the features to be observed. Then the etched features were flooded with copious amounts of AZ 4562 resist, which was then baked at 100 °C for one hour. The samples were mechanically polished at the cut, while the hardened resist was keeping the cross-section of the channels more or less intact. After polishing, the resist was removed with acetone.

Fig. 6. shows SEM images of Channel 3 (35 μm deep) and Channel 4 (36 μm deep) type test structures, etched for 35 minutes. The channel edges in both cases show an inflection and the width is larger than $2h + w$, where h is the etch depth and w is the initial width of the mask aperture. This suggests

This article has been accepted for inclusion in a future issue of this journal. Content is final as presented, with the exception of pagination.

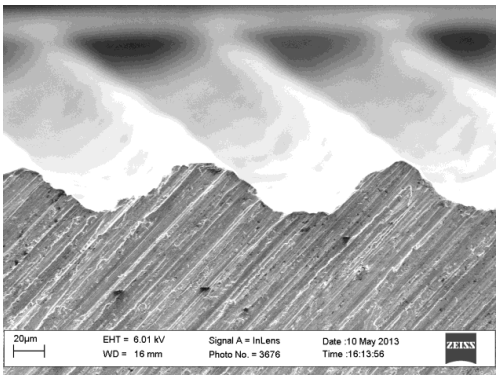

Fig. 7. SEM pictures of 33 μm deep (etched 35 min. at 50 °C) Channel 2 test structures. Channel 2 were obtained with 20 μm wide mask openings. The spacing between Channel 2 openings was 80 μm. The structures are intact but rounded, suggesting that the resist has delaminated but still stayed in place until the end.

that the resist has partially delaminated near the feature edges and let some etchant penetrate underneath. More accurate measurements with the stylus profilometer produced values for the average width of 219 μm for Channel 4 structures and 159 μm for Channel 3.

Channel 2 structures etched for 35 minutes (Fig. 7) shows a more drastic effect of the resist delamination during etching. The profile of the channels is quasi sinusoidal.

Fig. 8 shows SEM micrographs of the MFCs flowfield cross-section. The rough etched surface of the flowfield is also clearly visible in these micrographs. Interestingly, the etched profiles of the pillars show no inflection at all (compare with Fig. 6. and Fig. 7). Instead, the cross section of the profile has a sharp corner at the edge near the top of the pillar. The most likely explanation for this is that resist adhesion on a rough etched surface of the basin is better than on polished surface.

In their study of aluminum micromachining, Peixoto et al. [6] used a dicing machine to obtain high aspect ratio structures; 1.5 mm tall, 200 μm wide pillars. These were subsequently etched in a Type A (H_3PO_4-based) aluminum etchant in a combination of chemical and electrochemical etching, the details of which are not given. The process depends on the pillars being electrically isolated from each other, which is not generally possible in microfluidic applications.

Optical micrographs of the flowfield, taken after etching but before spraying with a jet of water, reveal a regular overhang of the photoresist (Fig. 9). The resist overhang is not deflected, as evidenced by the fact that focusing the microscope at higher magnifications did not reveal out-of-plane or sagging photoresist.

Since the developer we used (AZ 351B) is alkaline, it will slightly etch the aluminum wafer, and the alloying elements (Cu, Fe, Zn, Mg) will contaminate it. For this reason, a separate developer bath was be used. The etched depth is assumed to be only a few nanometers, and insignificant relative to structure depths.

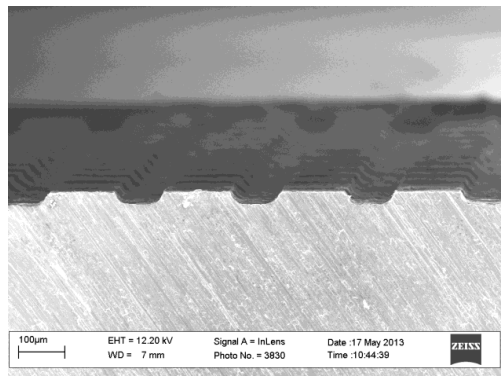

(a)

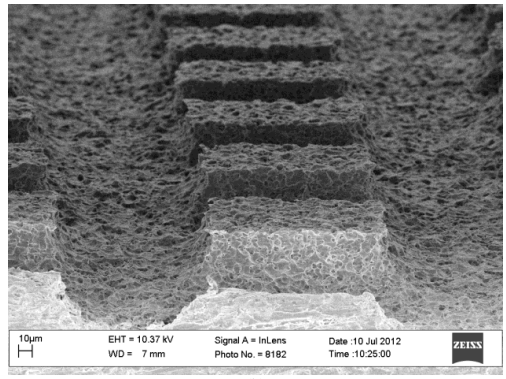

(b)

Fig. 8. SEM micrographs of MFC. (a) Flowfield at the bottom of a basin. (b) Close-up of flowfield, showing the roughness of the surface.

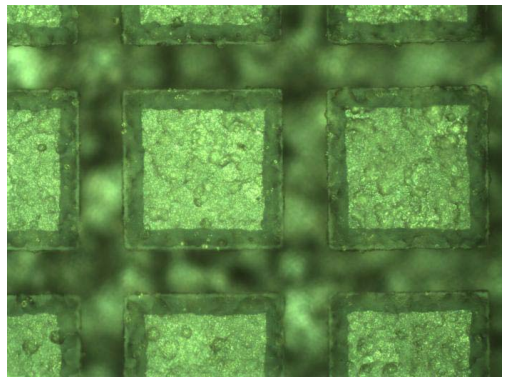

Fig. 9. Optical micrograph of MFC flowfield after etching, but before removal of AZ 5214 photoresist. The overhanging photoresist is clearly visible.

B. Micro Fuel Cell Results

Since the flowfield in the MFCs acts as a current collector, and contacting with the MFC chips is done between the back of the chips and the measurement jig's surface, it is

This article has been accepted for inclusion in a future issue of this journal. Content is final as presented, with the exception of pagination.

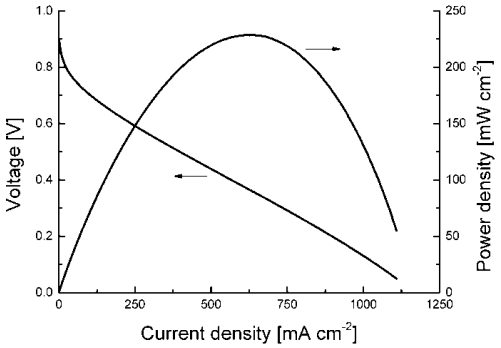

Fig. 10. Polarization curves obtained with oxygen as oxidant. The maximum current density obtained is 1109 mA cm^{-2}. The maximum power density is 228 mW cm^{-2}.

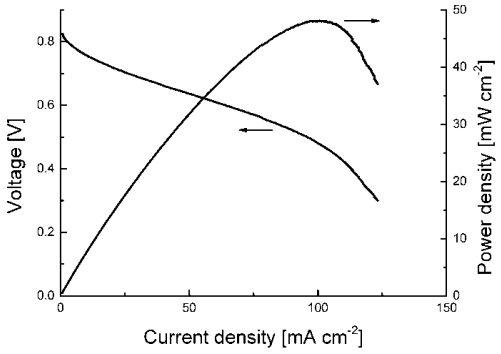

Fig. 11. Polarization curves obtained with artificial air as oxidant. A maximum current density of 123 mA cm^{-2} and a maximum power density of 48 mW cm^{-2} were obtained.

important that the back of the processed wafer remains as smooth as possible. To avoid etching this surface and to protect it from roughening, we spinned resist on the back of the wafer (Fig. 3a-c).

The through-holes for the reactant gases were drilled instead of etched, because an attempt at very long time etch, necessary to remove $\sim$ 800 μm of 6061 aluminum, caused catastrophic delamination of resist. It is also not clear how long such an etch step would have taken even if a suitable resist existed, because of the etch rate slow-down discussed in the previous subsection.

The depth of the basins and of the flowfield channels was selected so that the commercial carbon cloth would fit without too much compression.

Polarization curves indicate how much electrical current and power can be drawn from a fuel cell [9]. They are presented with oxygen as oxidant on Fig. 10, while those with artificial air are on Fig. 11. It can be seen that with oxygen very high power and current densities were reached due to the high conductivity of the aluminum chips. The current density at 0.3 V was 735 mA cm^{-2} and the maximum power density was 228 mW cm^{-2}. The maximum current density was 1109 mA cm^{-2}.

TABLE V
COMPARISON OF MFC WITH COMPETING DESIGNS

Research	Max. Current Density [mA cm^{-2}]	Max. Power Density [mW cm^{-2}]	Min. Sustained Current Density [mA cm^{-2}]	Reactants
This Work	1109	228	90	H_2/O_2
Kuriyama [18]	250	75	n/a	H_2/O_2
Yeom [19]	80	35	n/a	H_2/O_2
Kelley [20]	660	15	n/a	MeOH/Air, at 70ºC
Weiland [17]	500	220	n/a	H_2/Air 10 ms

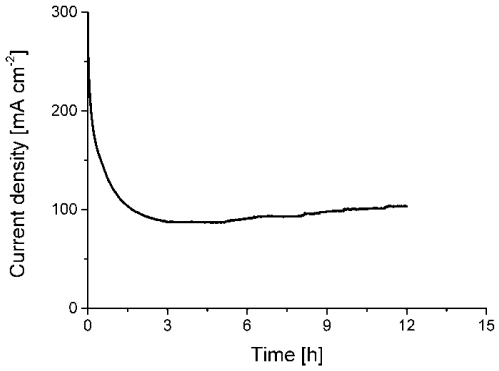

Fig. 12. Chronoamperometric measurement diagram. The current density stabilizes after about 3 hours and then slowly increases.

Table 5 lists some existing high-performance MFC results compared to ours. The design by Weiland et al. [17] produces power density comparable to the one in this work, but it was achieved for 10 ms intervals. It is remarkable that the other articles in the summary table do not mention chronoamperometric characterization.

When artificial air is used instead of oxygen, the performance of the MFC is substantially poorer as expected. The current density at 0.3 V is 123 mA cm^{-2} and the maximum power density is 48 mW cm^{-2}. Similarly, the open circuit voltage decreases from 900 mV to 820 mV.

For the artificial air case, there is a steeper voltage drop at high current densities ($>$ 100 mA cm^{-2}) than at lower current densities. This is caused by the consumption of oxygen which is required for the electrical current generation. As the current rises, the more depleted of oxygen the artificial air near the MEA surface becomes and the longer the distance oxygen has to diffuse to reach the MEA. This is seen as an extra resistance in the polarization curve called mass transfer resistance [21]. The measurement for the polarization curve was terminated after this limiting resistance was noticed. In the case of pure oxygen oxidant, this resistance is not seen even though the current is ten times larger, since the availability of oxygen is also much higher.

Stability of the MFCs was studied by keeping the voltage of the MFC at 0.6 V for 12 hours (Fig. 12). By measuring the current during this time, it can be concluded that after initial decrease in performance, the output current stabilized

This article has been accepted for inclusion in a future issue of this journal. Content is final as presented, with the exception of pagination.

around 100 mA cm^{-2}, which corresponds to output power of 60 mW cm^{-2}.

IV. Conclusion

Wet studied etching of 6061 aluminum alloy wafers and successfully fabricated micro fuel cells with good electrical performance. This is the first time, to the authors' knowledge, that bulk aluminum was lithographically patterned and etched for a MEMS application. The high electrical conductivity of aluminum is advantageous for MFCs where flowfields act as a current collectors. Bulk aluminum wet etch technology is able to achieve excellent performance with very simple equipment. The MFC characterization results shows very well functioning devices. Using a metal substrate such as aluminum, for MFCs, has an additional advantage compared to silicon: aluminum is ductile and can be compressed tightly. This is beneficial to minimize gas leaks and electrical contact resistance when the chips are stacked together.

Wet etching bulk aluminum presents a series of challenges: as Fig. 7 and 8 indicate, delamination of photoresist is a significant phenomenon in case of etch times longer than 20 minutes, and it will cause either a rounding of the microstructure edges, or a complete failure and detachment of the resist from the protected area. Such delamination was not seen with the rough aluminum surface obtained by previous etching (Fig. 9 and 10). This phenomenon, together with the isotropic profile and high roughness, makes it difficult to pattern small features.

Another challenge of wet etching aluminum alloys, specifically 6061, is the slowing of the etch rate with time, and the surface-formed non-etched products, which require cleaning. Conveniently, the cleaning consists of brief water spraying of the wafer. We have not, however, found a solution to speed up the etch rate in case of longer etch times. Agitation or a bubbler set-up may help in removing the non-soluble by-products and keep the etch rate steady. We did not explore the option of modifying the aluminum etchant.

The resulting roughening of the etched aluminum surface can be unacceptable in microfluidic applications where bonding is required, while it could be beneficial for others - for instance, if an increased surface area is desired.

In general, the ability to microfabricate fluidic devices from bulk aluminum goes beyond MFCs: polished aluminum plates could be made in almost any size, unlike other MEMS bulk materials. Using the methods described in this work, such large plates could be processed, as long as a suitably large area patterning is available.

Acknowledgment

The microfabrication effort took place in the Aalto Nanofab cleanroom.

References

[1] C. S. Effenhauser, A. Manz, and H. M. Widmer, "Glass chips for high-speed capillary electrophoresis separations with submicrometer plate heights," *Anal. Chem.*, vol. 65, no. 19, pp. 2637–2642, 1993.

[2] A. Y. Yi, Y. Chen, F. Klocke, G. Pongs, A. Demmer, D. Grewell, and A. Benatar, "A high volume precision compression molding process of glass diffractive optics by use of a micromachined fused silica wafer mold and low T_g optical glass," *J. Micromech. Microeng.*, vol. 16, pp. 2000–2005, Oct. 2006.

[3] H. Becker and L. E. Locascio, "Polymer microfluidic devices," *Talanta*, vol. 56, no. 2, pp. 267–287, 2002.

[4] S. Dey and K. S. Koul "Design and development of a surface micromachined push-pull-type true-time-delay phase shifter on an alumina substrate for Ka-band T/R module application," *J. Micromech. Microeng.*, vol. 22, no. 12, p. 125006, 2012.

[5] H. Becker, M. Arundell, A. Harnisch, and D. Hülsenberg, "Chemical analysis in photostructurable glass chips," *Sens. Actuators B*, vol. 86, nos. 2–3, pp. 271–279, 2002.

[6] A. C. Peixoto, A. F. Silva, N. S. Dias, and J. H. Correia, "Invasive neural electrodes structure fabrication based on aluminum wafers," in *Proc. 23rd Micromech. Microsyst. Eur. Workshop*, 2012 [Online]. Available: https://www.tu-ilmenau.de/mme2012/proceedings/

[7] K. R. Williams and R. S. Muller, "Etch rates for micromachining processing," *J. Microelectromech. Syst.*, vol. 5, no. 4, pp. 256–269, Dec. 1996.

[8] S. B. Lee, D. T. Mitchell, L. Trofin, T. K. Nevanen, H. Söderlund, and C. R. Martin, "Antibody-based bio-nanotube membranes for enantiomeric drug separations," *Science*, vol. 296, no. 5576, pp. 2198–2200, Jul. 2002.

[9] *Fuel Cell Handbook*, 7th ed., EG&G Tech. Services Inc. Morgantown, WV, USA, 2004.

[10] N.-T. Nguyen and C. S. Hwa, "Micromachined polymer electrolyte membrane and direct methanol fuel cells-a review," *J. Micromech. Microeng.*, vol. 16, no. 4, pp. R1–R12, 2006.

[11] G. Scotti, P. Kanninen, M. Mäkinen, T. Kallio, and S. Franssila, "Silicon nanograss as micro fuel cell gas diffusion layer," *Micro Nano Lett.*, vol. 5, no. 6, pp. 382–385, 2010.

[12] G. Scotti, P. Kanninen, T. Kallio, and S. Franssila, "Integration of carbon felt gas diffusion layers in silicon micro fuel cells," *J. Micromech. Microeng.*, vol. 22, no. 9, p. 094006, 2012.

[13] J. H. Joo and G. M. Choi, "Simple fabrication of micro-solid oxide fuel cell supported on metal substrate," *J. Power Sources*, vol. 182, no. 2, pp. 589–593, 2008.

[14] M. W. Moreau, *Semiconductor Lithography—Principles, Practices, and Materials*, New York, NY, USA: Plenum, 1988.

[15] C. Iliescu, F. E. H. Tay, and J. Miao, "Strategies in deep wet etching of Pyrex glass," *Sens. Actuators A, Phys.*, vol. 133, no. 2, pp. 395–400, 2007.

[16] C. Iliescu, J. Jing, F. E. H. Tay, J. Miao, and T. Sun, "Characterization of masking layers for deep wet etching of glass in an improved HF/HCl solution," *Surf. Coatings Technol.*, vol. 198, nos. 1–3, pp. 314–318, 2005.

[17] M. Weiland, S. Wagner, R. Hahn, and H. Reichl, "Design and evaluation of a passive self-breathing micro fuel cell for autonomous portable applications," *Int. J. Hydrogen Energy*, vol. 38, no. 1, pp. 440–446, 2013.

[18] N. Kuriyama, T. Kubota, D. Okamura, T. Suzuki, and J. Sasahara, "Design and fabrication of mems-based monolithic fuel cells," *Sens. Actuators A, Phys.*, vols. 145–146, pp. 354–362, Jul./Aug. 2008.

[19] J. Yeom, G. Z. Mozsgai, B. R. Flachsbart, E. R. Choban, A. Asthana, M. A. Shannon, and P. J. A. Kenis, "Microfabrication and characterization of a silicon-based millimeter scale, PEM fuel cell operating with hydrogen, methanol, or formic acid," *Sens. Actuators B, Chem.*, vol. 107, no. 2, pp. 882–891, 2005.

[20] S. C. Kelley, G. A. Deluga, and W. H. Smyrl, "Miniature fuel cells fabricated on silicon substrates," *AIChE J.*, vol. 48, no. 5, pp. 1071–1082, 2002.

[21] C. S. Kong, D.-Y. Kim, H.-K. Lee, Y.-G. Shul, and T.-H. Lee, "Influence of pore-size distribution of diffusion layer on mass-transport problems of proton exchange membrane fuel cells," *J. Power Sources*, vol. 108, no. 1, pp. 185–191, 2002.

Gianmario Scotti received the M.Sc. degree in electrical engineering from the University of Novi Sad, Novi Sad, Serbia, and pursued a career in information technology. He returned to science with his current Ph.D. work, which is focused on microfabrication, with a specialization in microfluidics and micro fuel cells. His current research interests include laser ablation and lithography techniques.

Petri Kanninen received the M.Sc. degree in chemistry from Helsinki University of Technology, Helsinki, Finland, in 2006. He is currently pursuing the Doctorate degree in physical chemistry. His current research interests include low-temperature fuel cells and electrochemical hydrogen production.

This article has been accepted for inclusion in a future issue of this journal. Content is final as presented, with the exception of pagination.

Tanja Kallio received the M.Sc. and D.Sc. degrees in chemical engineering from Helsinki University of Technology, Helsinki, Finland, in 1998 and 2003, respectively. She is with the Helsinki University of Technology (renamed Aalto University in 2010), working on electrochemical energy conversion and storage devices. Her current research interests include electrocatalysis of direct alcohol fuel cells and electrochemistry of electroactive materials for lithium ion batteries and super capacitors. Dr. Kallio has some 40 publications in peer-reviewed journals.

Sami Franssila received the B.Sc. and M.Sc. degrees in physics from the University of Helsinki, Helsinki, Finland, in 1985 and 1986, respectively, and the Ph.D. degree from the School of Electrical Engineering, Helsinki University of Technology, Helsinki, in 1995. He was a Research Scientist with the Technical Research Centre of Finland (VTT) Microelectronics section from 1986 to 1998 and a Visiting Scientist with IMEC, Heverlee, Belgium, from 1993 to 1994. He has been with Helsinki University of Technology (renamed Aalto University in 2010 university fusion) since 1998, where he is currently a Professor with the Department of Materials Science and Engineering. He has worked on CMOS, microelectromechanical systems, thin-film technology, and microfluidics. He holds three patents and has authored or coauthored 120 peer-reviewed journal articles and the textbook *Introduction to Microfabrication* (Wiley, 2010). His current research interests include materials and fabrication technologies for micro- and nanodevices.